Differences in Atmospheric Heat Source between the Tibetan Plateau–South Asia Region and the Southern Indian Ocean and Their Impacts on the Indian Summer Monsoon Outbreak

Yiwei ZHANG[1*], Guangzhou FAN[1,2], Wei HUA[1,2], Yongli ZHANG[1], Bingyun WANG[1], and Xin LAI[1]

1 *College of Atmospheric Sciences, Chengdu University of Information Technology/Plateau Atmosphere and Environment Key Laboratory of Sichuan Province, Chengdu* 610225

2 *Collaborative Innovation Center on Forecast and Evaluation of Meteorological Disasters, Nanjing University of Information Science &Technology, Nanjing* 210044

(Received April 22, 2016; in final form September 30, 2016)

ABSTRACT

In this paper, the NCEP–NCAR daily reanalysis data are used to investigate the characteristics of the atmospheric heat source/sink (AHSS) over South Asia (SA) and southern Indian Ocean (SIO). The thermal differences between these two regions and their influence on the outbreak of the Indian summer monsoon (ISM) are explored. Composite analysis and correlation analysis are applied. The results indicate that the intraseasonal variability of AHSS is significant in SA but insignificant in the SIO. Large inland areas in the Northern Hemisphere still behave as a heat sink in March, similar to the situation in winter. Significant differences are found in the distribution of AHSS between the ocean and land, with distinct land–ocean thermal contrast in April, and the pattern presents in the transitional period right before the ISM onset. In May, strong heat centers appear over the areas from the Indochina Peninsula to the Bay of Bengal and south of the Tibetan Plateau (TP), which is a typical pattern of AHSS distribution during the monsoon season. The timing of SA–SIO thermal difference turning positive is about 15 pentads in advance of the onset of the ISM. Then, after the thermal differences have turned positive, a pre-monsoon meridional circulation cell develops due to the near-surface heat center and the negative thermal contrast center, after which the meridional circulation of the ISM gradually establishes. In years of early (late) conversion of the SA–SIO thermal difference turning from negative to positive, the AHSS at all levels over the TP and SIO converts later (earlier) than normal and the establishment of the ascending and descending branches of the ISM's meridional circulation is later (earlier) too. Meanwhile, the establishment of the South Asian high over the TP is later (earlier) than normal and the conversion of the Mascarene high from winter to summer mode occurs anomalously late (early). As a result, the onset of the ISM is later (earlier) than normal. However, the difference in vorticity between early and late conversion only shows in the changes of strong vorticity centers' location in the upper and lower troposphere.

Key words: Tibetan Plateau, South Asia, southern Indian Ocean, atmospheric heat source, Indian summer monsoon, land–ocean thermal contrast

Citation: Zhang, Y. W., G. Z. Fan, W. Hua, et al., 2017: Differences in atmospheric heat source between the Tibetan Plateau–South Asia region and the southern Indian Ocean and their impacts on the Indian summer monsoon outbreak. *J. Meteor. Res.*, **31**(3), 540–554, doi: 10.1007/s13351-017-6042-5.

1. Introduction

Ye and Gao (1979) were the first to quantify the atmospheric heat source/sink (AHSS) over the Tibetan Plateau and the associated summertime heat effect of the region. Since then, the heat effect of the Tibetan Plateau has become an important focus for meteorologists worldwide. Chen and Li (1981, 1982) and Li and Chen (1983) calculated summertime AHSS over Asia. They found that the strongest heat center is located over an area ex-

Supported by the National Natural Science Foundation of China (91537214, 41275079, 41405069, 41305077, and 41505078), China Meteorological Administration Special Public Welfare Research Fund (GYHY201506001), Scientific Research Fund of Sichuan Education Department (16ZA0203), and Chengdu University of Information Technology Scientific Research Fund (J201516, J201518, and KYTZ201517).

*Corresponding author: sue.zhangyw@hotmail.com.

tending from the Bay of Bengal (BOB) to the north of Myanmar, and the heat center in northeastern Tibetan Plateau is a northern component of the strongest heat center. Luo and Yanai (1984) also calculated AHSS and further confirmed the above conclusion, based on observations over the Tibetan Plateau in 1979 obtained from the Qinghai–Xizang Plateau Meteorological Science Experiment. Jiang and Luo (1993) found that the active intraseasonal AHSS variability in Asia occurs over the area from northern BOB to the south of the Tibetan Plateau, corresponding well with the precipitation center. South Asia (SA) is located in the tropics, where surface sensible heat flux is large in spring and autumn. In summer, the Indian summer monsoon (ISM) brings abundant precipitation over this region and produces the strongest atmospheric heating in Asia for whole year due to the huge amounts of latent heat released during condensation–precipitation. In all of the studies mentioned above, meteorologists investigated the thermal effects of the Tibetan Plateau and South Asia separately, and mainly focused on the thermal effects of the Tibetan Plateau. However, on the planetary scale, the Tibetan Plateau and South Asia are two components of the same strong Asian heating center in summer, and therefore their thermal effects should be studied as an integrated system.

The ISM is a typical tropical monsoon system, which includes two distinct seasonal circulation patterns: outflow from the cold anticyclone over the continent in winter; and inflow to the warm cyclonic low-pressure center over the continent in summer (Ramage, 1971). The outbreak of the Asian summer monsoon occurs in the BOB first, then gradually moving northward and demonstrating a periodic feature (Pan and Li, 2006). The monsoon region experiences distinct dry and wet seasons following the beginning and end of the ISM. The correlation between the intensity of the ISM and precipitation over the monsoon region is high, with coefficients of greater than 0.99 (Yim et al., 2014).

The ocean–land thermal contrast is an important mechanism for the generation of monsoon. Essentially, the global monsoon system is the result of the atmospheric response to the intraseasonal variability of solar radiation over the land and ocean. Many previous studies (e.g., Luo and Zhang, 1991; He et al., 2007) have shown that the thermal forcing of the Tibetan Plateau and the zonal ocean–land thermal differences over East Asia and the Pacific region have considerable impacts on the East Asian monsoon system. Wu et al. (2011) investigated the features of surface sensible heat flux and wind fields in South Asia. They found that the zonal ocean–land thermal difference between the South Asian subcontinent and the ocean over the Arabian Sea and BOB is a critical factor for the formation of cyclones over the BOB in the pre-monsoon season. Wang and Wu (2008) found that differences in surface latent and sensible heat fluxes between the ocean and land are significant in the low-latitude region of South Asia—a pattern that greatly affects the low-level monsoonal circulation in the tropics. The above studies have revealed effects of the zonal ocean–land thermal differences over South Asia on the BOB monsoon. However, studies on the impacts of planetary-scale meridional thermal difference on the outbreak of the ISM are lacking. In this study, South Asia and the main body of Tibetan Plateau (TP) are treated as one region. The effects of the meridional thermal difference between this region and the Indian Ocean region in the Southern Hemisphere on the outbreak of the ISM are investigated.

2. Data and methodology

Daily horizontal winds, temperature, vertical velocity, and surface pressure, extracted from the NCEP–NCAR reanalysis database, with a resolution of 2.5° × 2.5°, for 1948–2013, are exploited to calculate the AHSS, by using the method proposed by Yanai et al. (1992).

The Webster–Yang index (WYI; Webster and Yang, 1992) is used to define the outbreak time of the ISM. Wang and Fan (1998) pointed out that this index not only covers the area of the ISM, but also affects the South China Sea and the Southeast Asia region. Meteorologists' understanding of the monsoons is not yet unified and, on this basis, how we delineate monsoon regions also differs. For this reason, we modify the ISM region during calculation of the WYI. Following Yim et al. (2014), a region is identified to be a monsoon region if the summertime precipitation in this region accounts for more than 55% of the annual total precipitation. A rectangular area over 10°–30°N, 70°–105°E is selected to represent the ISM region. The monsoon index (M) is expressed as

$$M = U_{850} - U_{200},$$

where U_{850} and U_{200} represent the zonal wind at 850 and 200 hPa, respectively.

Since the ISM is a cross-equator system, we take the TP and the subcontinent of SA as one source region of atmospheric heat in SA. Definition of the study regions is shown in Fig. 1a. Area A covers the TP (27.5°–40°N, 80°–100°E), and areas B1+B2 cover the SA. Note that area A (TP) is a subregion of B1, that is, the SA defined herein includes the TP; and the subcontinent of SA refers to B1+B2–A, namely, the SA exclusive of the TP.

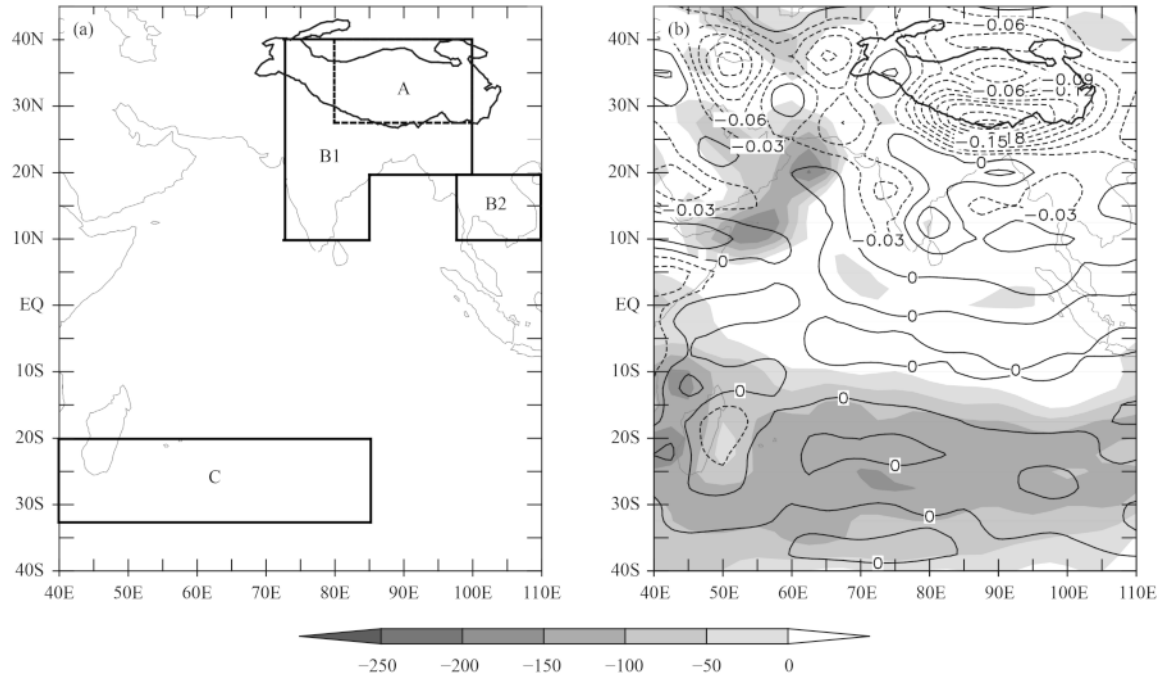

Fig. 1. The (a) research area and (b) distribution of summertime mean vertical velocity (contours; Pa s^{-1}) and integrated atmospheric heat source/sink (shaded; W m^{-2}) for the period 1948–2013. Region A denotes the Tibetan Plateau (TP); B1+B2 denotes South Asia (SA); and C denotes the southern Indian Ocean (SIO). Region A (TP) is a subregion of B1. The subcontinental SA covers B1+B2–A.

After the outbreak of the ISM, the ascending and descending branches, which are the components of the meridional circulation of the ISM system, maintain in response to the strong heat center over SA in the Northern Hemisphere and the cold center over the region from the Mascarene Islands to Australia in the Southern Hemisphere (Pan and Li, 2006). Based on distributions of multi-year average vertical velocities and AHSS, both after vertical integration during the monsoon season (Fig. 1b), and considering the fact that the center of the Mascarene high is located around 30°S, 45°E in summer (Cui and Yang, 2005), we select the area over 20°–32.5°S, 40°–85°E, that is, area C in Fig. 1a, in the southern Indian Ocean (SIO), for detailed study. A thermal-difference index is proposed to quantify the meridional thermal difference between SA (or TP) and SIO. The index is expressed as

$$\Delta\langle Q_1\rangle = \langle Q_1\rangle_{\text{area}} - \langle Q_1\rangle_{\text{SIO}},$$

where $\langle Q_1\rangle_{\text{area}}$ is the domain-averaged and vertically integrated AHSS. The subscript "area" can be replaced by SA or TP.

3. Characteristics of AHSS in SA and SIO

3.1 *Spatiotemporal variability*

The vertically integrated AHSS presents significant intraseasonal variability over SA, whereas the variability is relatively small over the SIO (Fig. 2). Over the TP, the maximum AHSS (~140 W m^{-2}) occurs in the 34th pentad, and the minimum value (–100 W m^{-2}) occurs in the 67th. The heat sink turns to a heat source around the 15th pentad, and the reversal from heat source to sink occurs around the 53rd pentad. In SA, the maximum heat source of around 640 W m^{-2} appears around the 41st pentad, which lags behind the occurrence of the maximum heat source in the TP by 7 pentads. This is attributed to the release of huge amounts of latent heat accompanied by the ISM and precipitation over the subcontinent of SA. The release of latent heat associated with monsoon

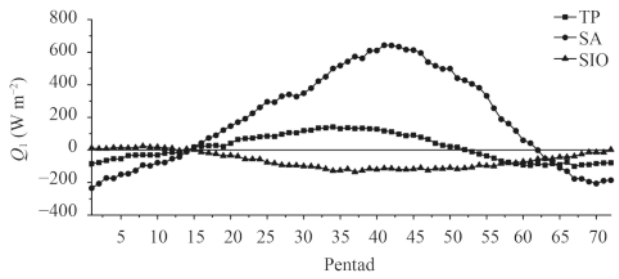

Fig. 2. Pentad time series of multi-year average atmospheric heat source (Q_1; W m^{-2}) for the period 1948–2013. The lines with square, circular, and triangular data points represent the main body of Tibetan Plateau (TP), South Asia (SA), and southern Indian Ocean (SIO), respectively.

precipitation is the major contributor to the atmospheric heat source in summer over SA. The strongest heat sink occurs in the 1st pentad, with the maximum value reaching –230 W m^{-2}. The heat sink turns to a heat source in SA at approximately the same time as in the TP, and the reversal from heat source to sink occurs around the 62nd pentad. Over the SIO, the maximum heat source (23 W m^{-2}) occurs in the 8th pentad, and the heat sink reaches its maximum value (–136 W m^{-2}) around the 37th pentad. The heat source turns to a heat sink in the 15th pentad, and the heat sink turns to a heat source in the 72nd pentad.

In order to investigate the impact of thermal differences between SA and SIO on the outbreak of the ISM, we analyze the spatial distribution characteristics of the springtime vertically integrated AHSS over the TP–subcontinental SA–SIO region. In March, the AHSS presents a positive–negative–positive–negative pattern from north to south over SA and SIO (Fig. 3a), while weak heat sources occur over the subcontinent of SA and the TP. The heat source is stronger in western TP than in eastern TP, and a weak heat sink occurs over the north of TP. A relatively strong heat sink occurs over the Arabian Sea and northwestern BOB because of the lower sea surface temperature (SST) over these areas induced by the upwelling of cold ocean water, which is caused by the zonal inhomogeneity of surface sensible heat flux in springtime over SA (Wu et al., 2011). The equatorial region and the SIO are regions of heat source, whereas the SIO to the south of 25°S is a heat sink region. All of these characteristics still display the wintertime thermal feature. In April (Fig. 3b), the atmospheric heat source intensifies over SA, and a maximum heat center appears to the south of the TP and the Indochina Peninsula. These heat centers are associated with the latent heat release of precipitation (He et al., 2011). The Arabian Sea and northwestern BOB are still heat sink regions, although the intensity of the heat sink decreases and the area of heat source in the SIO extends northward. In May (Fig. 3c), the atmospheric heat sources over SA further intensify, whereas a weak heat sink still remains in the Arabian Sea; heat sources of various intensity are found over the entire BOB; and the heat source in the SIO further intensifies and extends northward, starting to present some features of the summertime heat source distribution. In the following analysis, we focus on the situation in April, which is a representative month of pre-onset transition.

3.2 *Temporal relationship between the thermal effects of the TP and SA*

The TP is a major contributor to the springtime heating effect of SA. Here, we discuss the temporal relationship between the heating effect over the TP and that of SA and SIO during the transitional period before the outbreak of the summer monsoon. Figure 4 shows the spatial distributions of homochromous and lagged correlation coefficients (1- and 2-pentad leading) between the heat sources over the TP and entire SA region during pentads 13–24 (March–April). The homochromous correlation is the highest, followed by the 1-pentad leading correlation, and the 2-pentad leading correlation is the weakest. Looking at the spatial pattern, significant positive correlation is found over the entire SA, except western TP and part of the Indian Peninsula, with a value of 0.661 at the 99% confidence level. In contrast, the negative correlation is found over southern Arabian Sea, equatorial eastern Indian Ocean, and the Mascarene region in the Southern Hemisphere. The above results indicate that, in the transitional season before the outbreak of the monsoon, the intensified atmospheric heat source over the TP is favorable for intensification of the heat source in SA and the conversion from a heat source to a heat sink over the Mascarene region. Apparently, the heating condition in the TP can influence the thermal condition in subcontinental SA.

One possible reason for the significant relationship

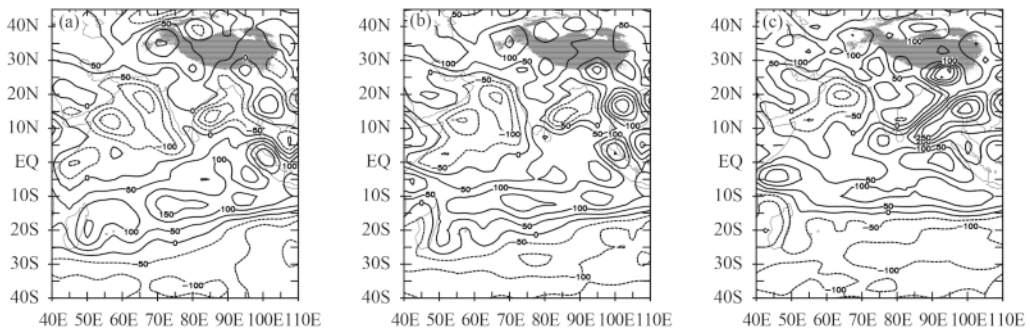

Fig. 3. Spatial distributions of multi-year average vertically integrated atmospheric heat source (W m^{-2}) in (a) March, (b) April, and (c) May from 1948 to 2013.

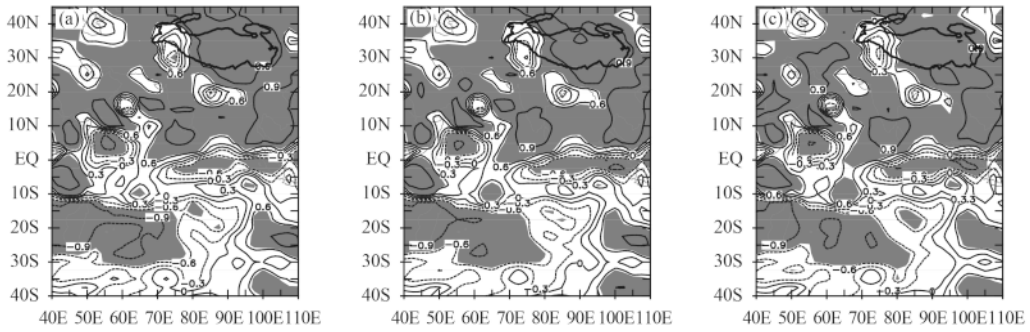

Fig. 4. (a) Homochromous, (b) 1-pentad leading, and (c) 2-pentad leading correlation distributions of the atmospheric heat source in the TP and the entire region (shaded areas indicate values significant at the 0.01 level).

between the atmospheric heat source in the TP and the subcontinent of SA is that, because of the high elevation of the TP, this region is extraordinarily efficient in heating the atmosphere. The air column above this region is much shallower than other places, and the TP can directly increase the temperature of the mid troposphere. Thus, the atmospheric heat source above the TP is highly sensitive. However, for the subcontinent of SA, the air column is deeper than the TP's, owing to its lower topography, so the heating effect is weaker. Suppose that the TP and the subcontinent of SA heat the atmosphere at the same level, the latter would need more time than the former. However, because of the limited resolution of reanalysis data, it is difficult to identify a specific region's heating effect. In addition, this study focuses on planetary-scale thermal and dynamical attributes of the atmosphere over the study domain. All in all, the TP and the subcontinent of SA will be investigated as an integrated area (SA) in the present work. In view of the outstanding role played by the TP, the thermal contrast between the TP and the SIO and related effects will be in particular explored in Sections 4 and 6 of this paper.

4. Thermal differences between SA and the SIO in spring

The WYI (Webster and Yang, 1992) is used to quantify the outbreak time of the ISM. When the WYI turns positive, it denotes the outbreak of the ISM. Likewise, when the WYI turns negative, it indicates the end of the ISM. The average time for the outbreak of the ISM is pentad 32.7 in Mumbai, India (Kumar et al., 1999). Xu and Qian (2006) calculated the WYI for the previous 40 years and determined that the time of ISM outbreak is pentad 28.2. They also suggested that the outbreak time of the ISM determined according to the WYI is earlier than normal. In the present study, we derive that the outbreak time of the ISM is pentad 29.8, which is consistent with the results of previous studies.

The thermal difference between SA and SIO can to a certain degree reflect the meridional ocean–land thermal difference over this region. The pentad time series of the thermal difference between SA and SIO, and that between TP and SIO, and the WYI, are shown in Fig. 5. The SA–SIO thermal difference and intensity of the heat source in SA reach their maximum values simultaneously in the 41st pentad, when the thermal difference can be greater than 755 W m^{-2}. The thermal difference and intensity of the heat source also reach their minimum values simultaneously, in the 1st pentad, when the thermal difference is –245.7 W m^{-2}. The SA–SIO and TP–SIO thermal differences both turn positive in the 15th pentad, and turn negative in the 64th pentad. The TP–SIO thermal difference reaches its maximum (268.8 W m^{-2}) in the 34th pentad, which is also the time when the heat source intensity in the TP reaches its peak. The minimum thermal difference (–95.4 W m^{-2}) occurs in the 1st pentad, which lags behind the occurrence of the maximum heat sink intensity by 6 pentads. The thermal difference turns negative in the 59th pentad. The outbreak time of the ISM is determined as the 30th pentad, and the end time as the 57th pentad, based on the WYI; and the time when the thermal difference turns positive leads the outbreak time of the monsoon by approximately 15 pentads. Furthermore, at the time of monsoon outbreak,

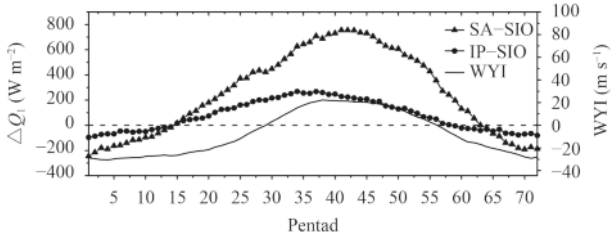

Fig. 5. Pentad time series of the multi-year average thermal difference (ΔQ_1; W m^{-2}) between SA and SIO (triangles), between TP and SIO (circles), and the WYI (solid line with no markers; m s^{-1}) from 1948 to 2013.

the intensification of the thermal differences between the TP and SIO, and between SA and SIO, both experience a short moderate period, with values of 202 and 432 W m^{-2}, respectively. After the outbreak of the ISM, the SA–SIO thermal difference rapidly intensifies due to the release of huge amounts of latent heat flux associated with monsoon precipitation.

Figure 5 shows the intraseasonal changes in the vertically integrated thermal difference and the monsoon. We focus on the heating and thermal differences at various levels in the following discussion. As shown in Fig. 6a, the atmospheric heating above the TP decreases with height. The maximum heating occurs near the surface at around 600 hPa, and the heating decreases significantly within 300–200 hPa. The heat source turns to a heat sink within 250–200 hPa, and reaches its minimum value at 100 hPa. In SA, the atmospheric heating is intense at 700 hPa and below, and reaches maximum heating near the surface at 1000 hPa. No large changes in the heating can be found between 800 and 300 hPa, but significant decreases can be found above 300 hPa. The heat source turns to a heat sink within 150–100 hPa. The vertical distribution of the atmospheric heat source in the SIO is opposite to that over the TP and subcontinental SA. The atmospheric heating in the SIO decreases with height at lower levels, and then increases with height at higher levels. Due to the influence of the underlying ocean surface, the atmospheric heating is intense in the surface layer. However, the heat source rapidly turns to a heat sink at around 900 hPa. The intensity of the heat sink intensifies gradually between 850 and 200 hPa, but decreases dramatically above 200 hPa and turns to a heat source at around 150 hPa. Thermal differences at various levels between SA and SIO are shown in Fig. 6d. The data clearly show that the thermal difference decreases with height and the maximum difference occurs at the surface. The thermal difference decreases rapidly between 925 and 600 hPa, but changes little between 600 and 250 hPa. The thermal difference quickly decreases above 200 hPa and turns negative at about 150 hPa.

The above analysis reveals seasonal variability of the thermal difference between SA and SIO. Next, we discuss the interannual variability of the timing of monsoon outbreak and changes in the thermal difference. Figure 7a presents a scatter plot of the thermal difference conversion time and monsoon outbreak time. The size of each individual dot indicates the frequency of its corresponding point, which ranges from 1 to 4. It is found that the thermal difference conversion time and monsoon outbreak time are both later than normal in 14 yr (quadrant Ⅰ), and both earlier than normal in 13 yr (quadrant Ⅲ). There are 16 yr when the thermal difference turns earlier than normal but the monsoon outbreak time is later than normal (quadrant Ⅱ). Meanwhile, the thermal difference turning later but the monsoon outbreak turning earlier takes place in 23 yr (i.e., quadrant Ⅳ). In total, positive correlation between the thermal difference conversion time and monsoon outbreak time occurs in 27 yr, and negative correlation in 39 yr, which surpasses 60% of the whole study period. Thus, this negative correlation is considered as a valuable result in this study. The correlation coefficient between the two time series is –0.208, statistically significant at the 0.1 level. Note that the scattering of the thermal difference conversion time is larger than that of the monsoon outbreak time, and shows larger interannual variability.

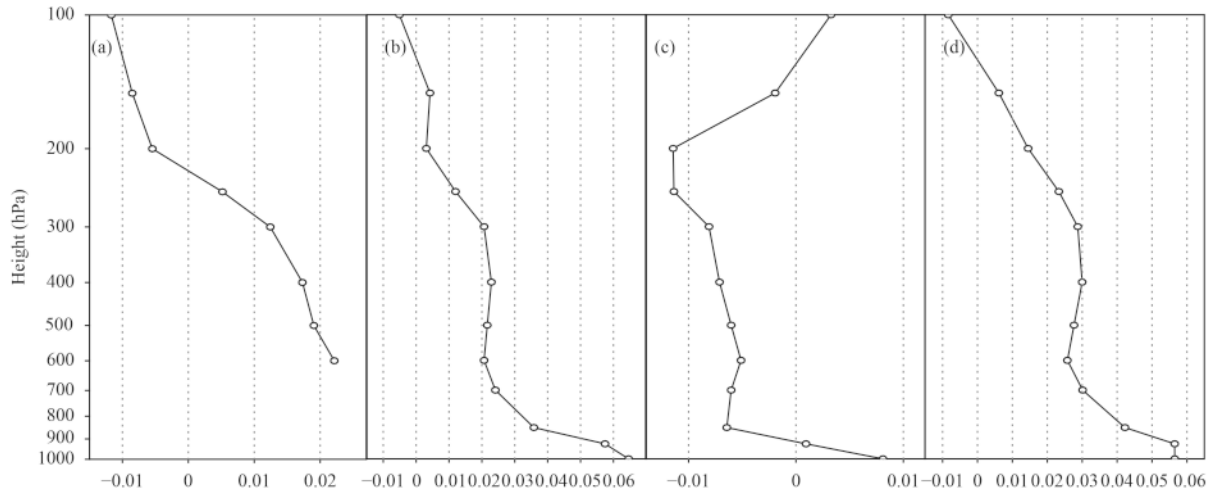

Fig. 6. Multi-year average vertical profiles of atmospheric heat source in (a) the TP, (b) SA, and (c) SIO, and (d) the difference between SA and SIO (K s^{-1}) from 1948 to 2013.

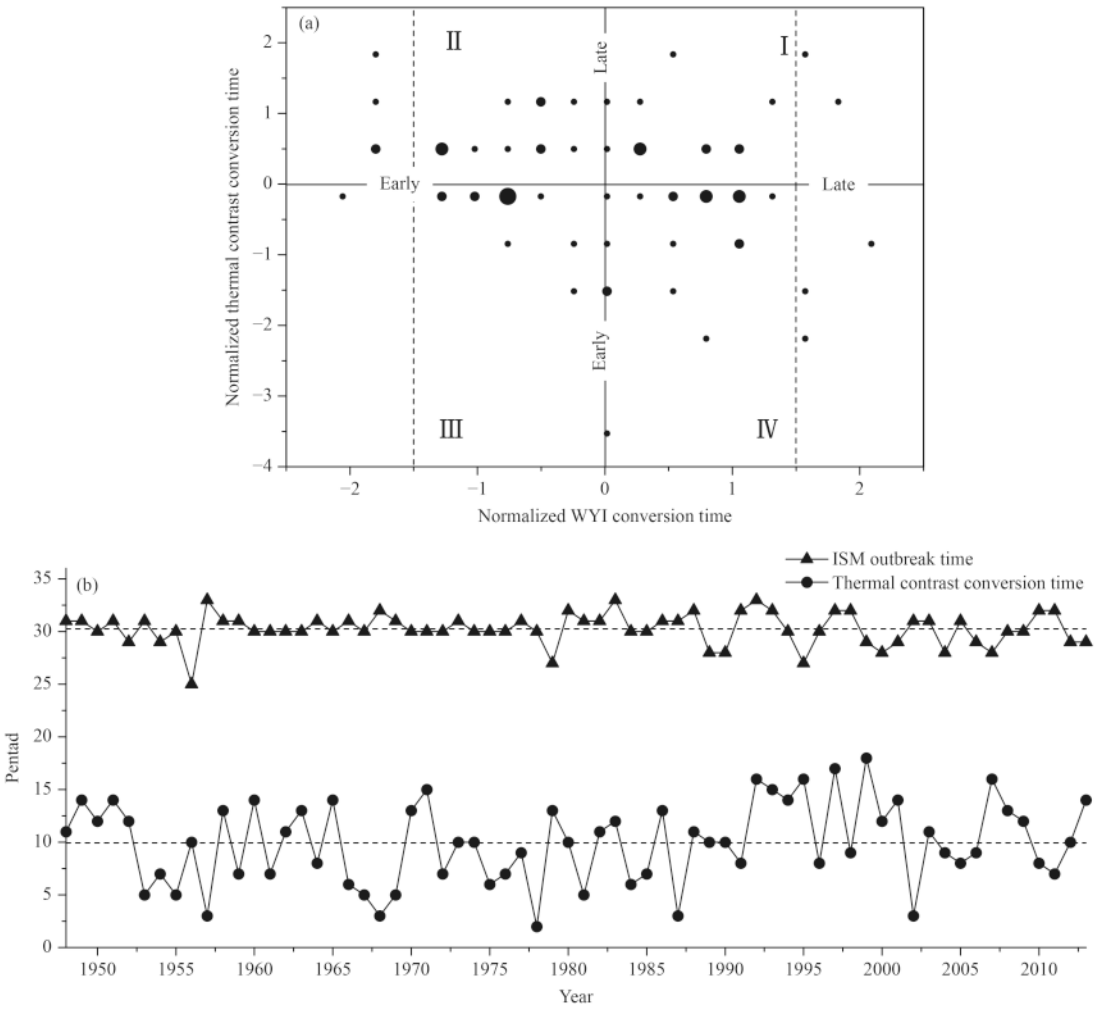

Fig. 7. Scatter plots of (a) the annual standardized and (b) pentad-sequence (pentad) conversion time of the atmospheric thermal contrast between SA and SIO and those of the onset time (defined by WYI) of the Indian summer monsoon (ISM) for the period 1948–2013. The size of the dots in (a) indicates the frequency, which ranges between 1 and 4, with 1 being the smallest dot size; the correlation coefficient between the two sequences in (a) is –0.208, which is significant at the 0.1 level; and the dashed lines in (b) indicate the average time of the thermal conversion and the monsoon onset, respectively.

Figure 7b indicates that the earliest time for the thermal difference between SA and SIO to turn from negative to positive is the 2nd pentad (in 1978), and the latest conversion time is the 18th pentad (in 1999). The earliest ISM outbreak time occurs in the 26th pentad (in 1956) and the latest outbreak time in the 33rd pentad (in 1957, 1983, and 1992). The conversion time for the SA–SIO thermal difference displays a distinct delaying trend since the 1990s, while the Indian monsoon outbreak time demonstrates a more significant interannual oscillation. The above results show clearly that large interannual variability exists in the SA–SIO thermal difference conversion. The earliest conversion time occurs in January, and the latest at the end of March, spanning a three-month period. In contrast, the interannual variability of the ISM outbreak time is relatively small. The earliest outbreak time occurs in May, and the latest in early June, spanning only a one-month period.

5. Physical process of the influence of the thermal difference between SA and SIO on ISM outbreak

The onset of the ISM is a progressive procedure that starts in the BOB in the 25th pentad, with the monsoon then expanding eastward and northward from the Southern Hemisphere (Liu et al., 2015). In Fig. 7b, the time at which the SA–SIO thermal contrast turns positive is found to lead the outbreak of the ISM by about 15 pentads. This time gap is partly due to the monsoon index calculation. To obtain accurate onset time, we utilize the WYI, which only calculates the Northern Hemispheric

monsoon region. Then, the particular physical process between these two times is investigated in this section.

As we know, the land–ocean thermal difference is the most important factor in monsoon formation. Therefore, with reference to Fig. 8, we can identify the physical mechanism involved in how the SA–SIO thermal contrast influences the ISM outbreak. In the 14th pentad, one pentad before the SA–SIO thermal difference turns positive, the Hadley circulation dominantly controls the whole tropical area, both in the Northern and Southern Hemispheres. The atmospheric circulation matches the thermal distribution perfectly, in which there is ascending motion in the heating area and descending motion in the cooling area. At the same time, the AHSS shows a "negative–positive–negative–positive–negative" distribution from north to south. However, in particular, there are two heating centers that appear above the TP, from the ground and at the upper-level atmosphere. Furthermore, the strongest thermal difference center is found at the same location. The subtropical Northern Hemisphere shows a heating effect in the near-ground layer; however, the AHSS there is smaller than in the SIO region. In the 15th pentad, when the SA–SIO thermal contrast turns positive, the Hadley circulation still controls the tropical region. Over the TP, the heating center and thermal difference center grow stronger and higher. Although the thermal difference between the subtropical Northern Hemisphere and the SIO is negative at this time, the heating effect of the whole SA region surpasses that in the SIO region. In the 16th pentad, one pentad after the thermal contrast turns positive, the AHSS of the subtropical Northern Hemisphere develops higher and stronger. Also, the thermal difference between this area and the SIO turns positive progressively. Owing to this change in the heating distribution, an ascending branch of vertical circulation appears in the same region. Therefore, the pre-monsoon circulation cell is formed. However, the Hadley circulation is still the dominant system in the tropical region, and the descending branch follows the cooling distribution well. Once the SA–SIO thermal contrast turns positive, the heat sink center is gradually replaced by a heat source in the Northern Hemispheric subtropics. At the same time, the pre-monsoon circulation cell grows to a higher (600 hPa) level, and the descending branch of the Hadley circulation is pushed northward.

In the 24th pentad, there is still a small heat sink region within 800–600 hPa over 10°–20°N, and a negative thermal difference center in the north of this heat sink center. This negative center offers the necessary thermal condition for the descending branch of the pre-monsoon cell. Therefore, in the 26th pentad, when the mid-level heat sink still exists but the negative thermal contrast center disappears, the pre-monsoon cell breaks and is replaced by the ascending branch of the Hadley circulation. The descending branch is located at the mid–upper levels in the TP's south side. In the 29th pentad, one pentad before ISM onset, the Northern Hemisphere area shows a relatively strong heat source. The most intensive heat centers appear in the mid-level at about 10°N and the TP. The greatest thermal difference center appears in the middle atmosphere at 10°N. The Northern Hemisphere region north of 40°N is controlled by ascending flow. North of 20°S, a strong cooling effect is found, resulting in a significant descending branch. In the 30th pentad, the ISM outbreak pentad, those heat source centers and thermal contrast centers grow bigger and stronger, as does the ascending flow. The ascending flow in the northern subtropics separates in two directions at the top of the troposphere, north and south, and then descends north of 40°N and south of 20°S. However, in the 31st pentad, one pentad after the ISM onset, the descending flow is replaced by the ascending flow around 40°N. In the 33rd pentad, the ascending flow basically travels south at the upper level, which generates the vertical-meridional monsoon circulation.

6. Mechanism by which the thermal difference between SA and SIO influences ISM outbreak in spring

6.1 *Thermal forcing effects*

To further explore the mechanism by which the conversion time of the thermal difference between SA and SIO influences the outbreak of the ISM, we first calculate the difference in the atmospheric heat source between SA and SIO, and then standardize the results. Since the ISM is affected by many factors (Ding and Murakami, 1994), we select a relatively strict criterion for the purpose of maximizing the influence of the thermal contrast between SA and SIO. Years with a standard deviation smaller than –1.5 (larger than 1.5) are identified as typically early (late) thermal difference conversion years. Five years (1957, 1968, 1978, 1987, and 2002) are identified as early conversion years, and another five years (1992, 1995, 1997, 1999, and 2007) as late conversion years (Fig. 7b). The average outbreak time of the ISM is the 31st pentad in years of early conversion; whereas, in years of late conversion, the average outbreak time is the 28th pentad. To explore the mechanism by which early and late thermal difference conversions influence the outbreak of the monsoon, we analyze the conversion of the atmospheric heat source and vertical

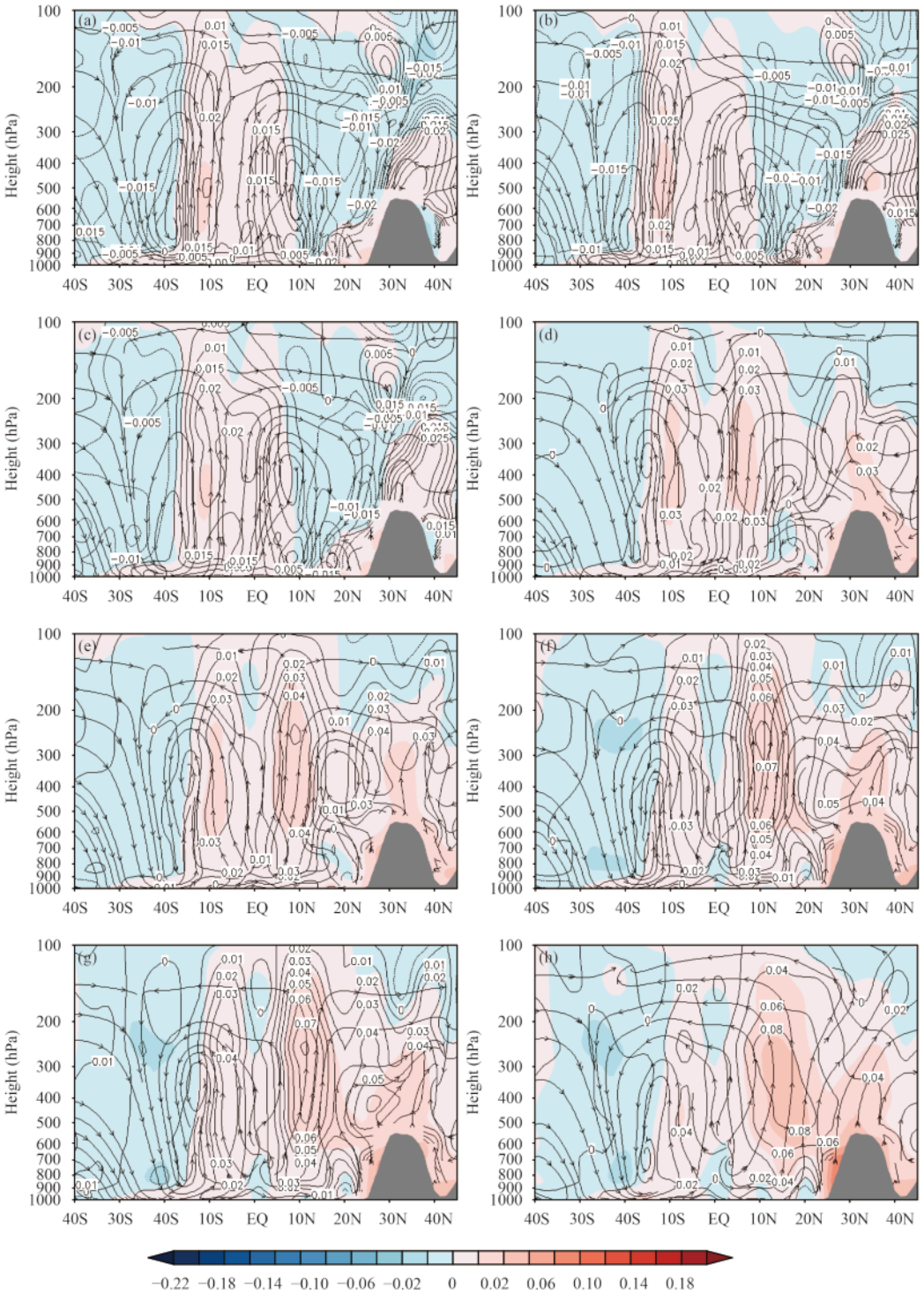

Fig. 8. Multi-year average vertical-meridional distributions of stream line, atmospheric heat source/sink (shaded; W m^{-2}), and the thermal difference (contours; W m^{-2}) with the southern Indian Ocean over 80°–100°E. (a) Pentad 14, (b) pentad 15, (c) pentad 16, (d) pentad 24, (e) pentad 26, (f) pentad 29, (g) pentad 30, and (h) pentad 33.

velocity.

Because of its unique topography, the TP is highly sensitive to the intraseasonal variation of solar radiation. The ascending branch of the meridional monsoonal circulation is located above the TP and its surrounding areas, and the descending branch is located over the Mascarene region. For this reason, we focus on the conversion of the atmospheric heat sources at various vertical levels over the TP and SIO. Figure 9 presents time–height cross-sections of the atmospheric heat source over

the TP and SIO. The dashed vertical lines in the figure indicate the average conversion time across all levels. Considering the overall conversion of the atmospheric heat source at all levels, it is found that, in years of early conversion, the heat source at all levels over the TP turns positive in the 28th pentad (Fig. 9a); in the surface layer, the heat source turns positive around the 10th pentad. In the SIO region, the atmospheric heat source turns completely negative around the 24th pentad, while the heat source at higher levels turns to heat sink around the 15th pentad (Fig. 9d). In years of late conversion, the atmospheric heat source over the TP turns completely positive in the 27th pentad (Fig. 9b), while in the surface layer the heat source turns positive around the 5th pentad. Over the SIO, the atmospheric heat source turns negative around the 16th pentad, while the heat source at higher levels turns to heat sink around the 12th pentad. In both early and late years of SA–SIO thermal difference conversion, the atmospheric heat source in the TP first turns positive at the surface, and then gradually turns positive with height; in the SIO, the atmospheric heat source first turns into heat sink at upper levels, and then gradually at lower levels. By comparing the situation between early and late conversion years, large differences can be found in the timing of conversion among different levels. Differences in the time of conversion from negative to positive over the TP are relatively small, and the general conversion time in early conversion years is one pentad earlier than in late years. In contrast, large differences exist in the conversion time over the SIO. The time of conversion in early years is eight pentads earlier than in late years.

The above section analyzes the heat source conversion at various levels over SA and the SIO in early and late years of thermal difference conversion in the two regions. Next, we explore the mechanism by which abnormal thermal effects influence the outbreak of the ISM, based on thermal adaption theory. Atmospheric thermal forcing is an important factor driving general atmospheric circulation. Anomalies in the spatial distribution of atmospheric thermal forcing often result in anomalous atmospheric circulation. Wu and Liu (2000) revealed the

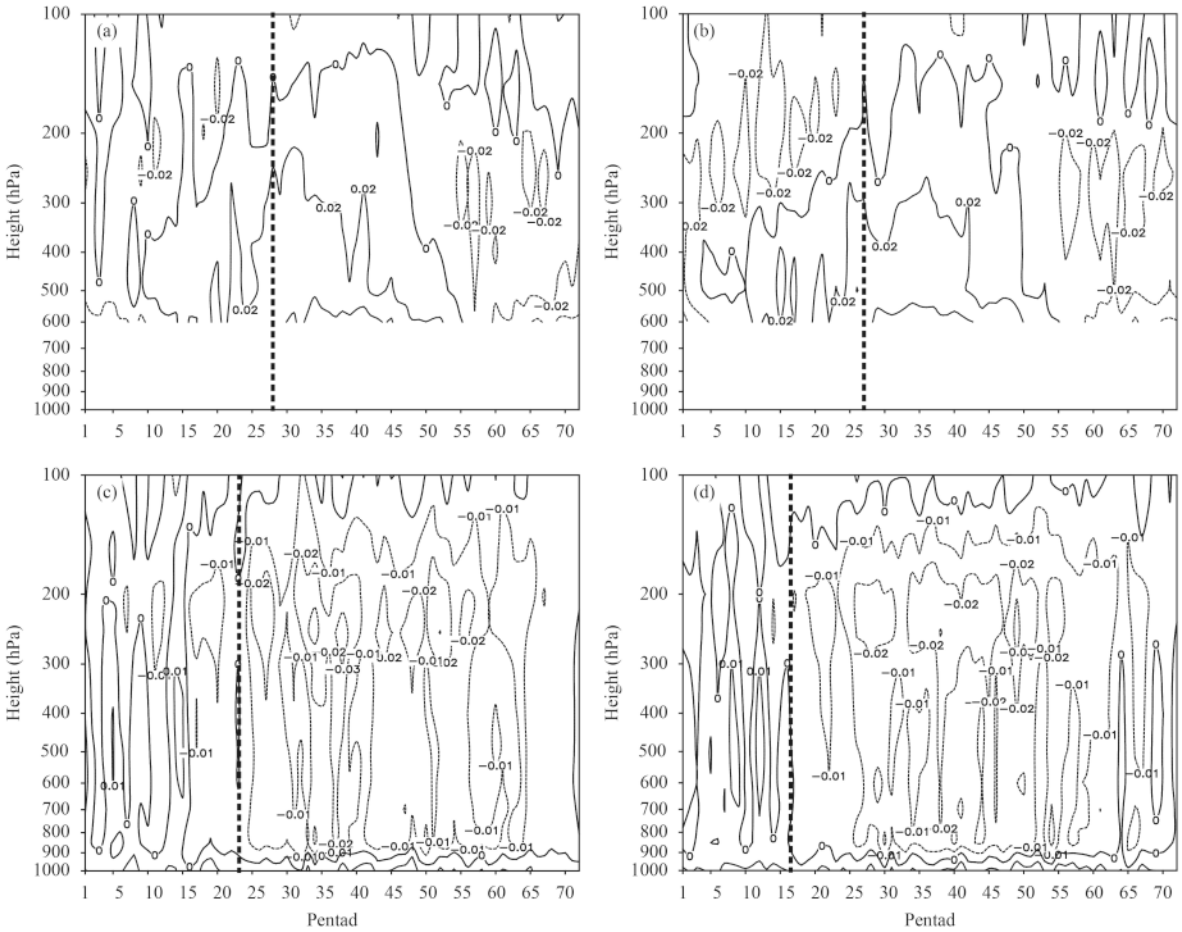

Fig. 9. The height–time variation by pentad of the atmospheric heat source (W m^{-2}) in (a, c) early and (b, d) late years of the thermal difference conversion over (a, b) the TP and (c, d) the SIO. The dashed lines indicate the conversion date.

mechanism involved in the atmospheric circulation response to thermal effects, based on the nature of the potential vorticity, that is, thermal adaption theory: local heating can lead to strong ascending motion in the same area, which behaves like a suction pump that produces convergence at lower levels and divergence at upper levels. In contrast, effects of an atmospheric heat sink can lead to strong descending motion, which produces divergence at lower levels and convergence at higher levels. Figure 10 presents time–height cross-sections of vertical velocity over the TP and SIO for early and late years of SA–SIO thermal difference conversion. Apparently, the change features are similar to those of the atmospheric heat source. In early thermal difference conversion years, ascending motion occurs around the 18th pentad over the TP surface, and the ascending branch completely establishes in the 29th pentad (Fig. 10a). In the SIO, a descending branch establishes around the 24th pentad. In late thermal difference conversion years, the vertical velocity over the TP (Fig. 10b) becomes positive around the 25th pentad, which is 4 pentads earlier than in early thermal difference conversion years, but the ascending motion at lower levels is slightly weaker. In the SIO region (Fig. 10d), weak descending motion occurs at middle levels in as early as the 10th pentad, but the descending branch does not completely establish until the 16th pentad, which is 8 pentads earlier than in early years of thermal difference conversion. In both early and late years, the vertical velocity over the TP always gradually changes from descending to ascending from lower levels upwards. In the SIO region, descending motion first occurs at middle levels, and then gradually propagates to lower levels. The evolution of vertical motion over the TP and SIO is similar to that of the atmospheric heat source. In summary, the time when ascending/descending motion establishes over the TP and SIO is affected by the thermal conversion time. In early and late years, an abnormal time of thermal conversion affects the establishment time of the ascending/descending motion over the TP and SIO, which is eventually reflected in an abnormal outbreak time of the ISM. This is also the reason why the conversion time of the SA–SIO thermal differ-

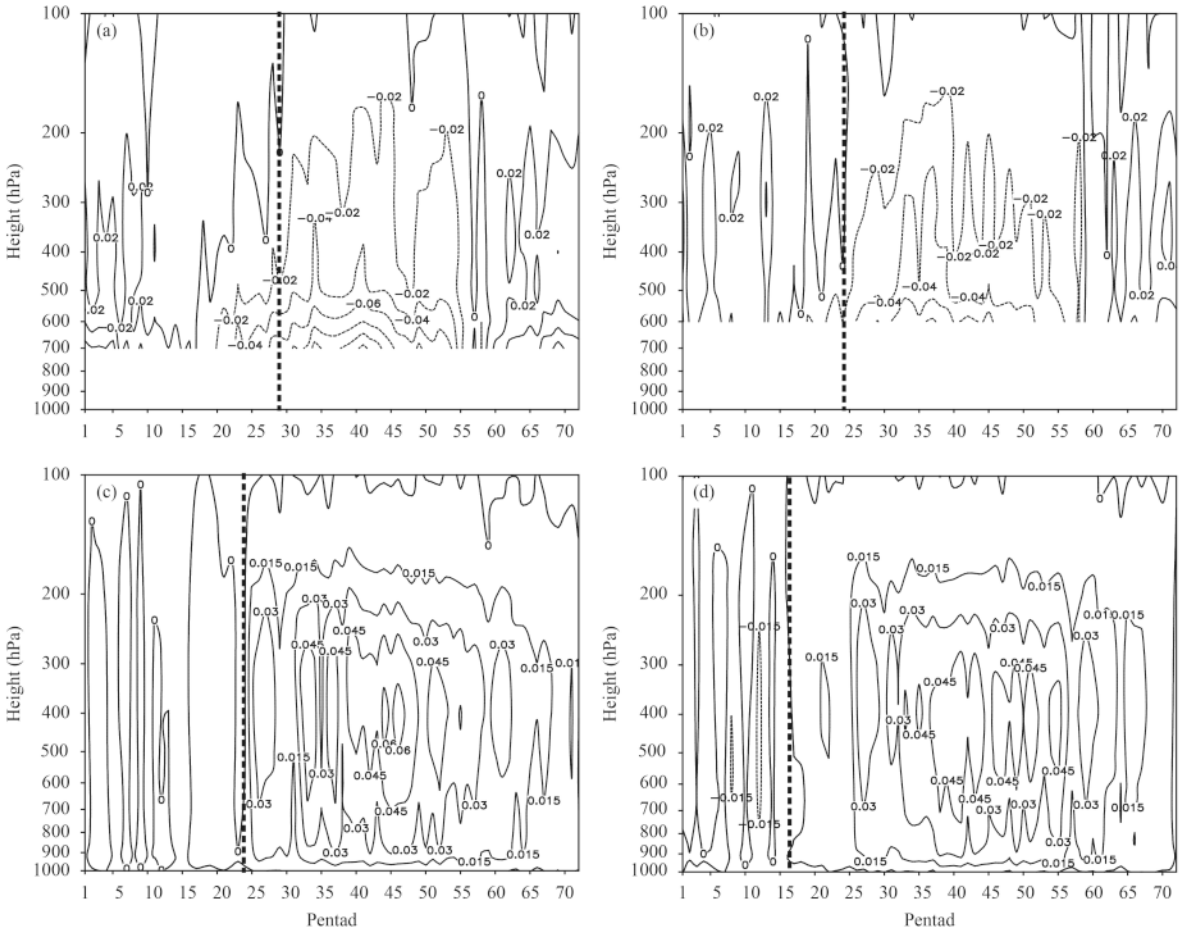

Fig. 10. Height–time cross-sections of pentad-averaged vertical velocity (Pa s^{-1}) in (a, c) early and (b, d) late years of thermal difference conversion over (a, b) the TP and (c, d) the SIO. The dashed lines indicate the conversion date.

ence is negatively correlated with the outbreak time of the ISM (Fig. 7).

After the discussion on the basis of thermal adaption theory, the most direct appearance of the annual land–ocean thermal contrast is shown in Fig. 11. In early conversion years, the atmospheric heat source difference between the TP and SIO turns positive in May (16th pentad), on average across all levels. Furthermore, the difference reaches its peak value (307 W m^{-2}) in the 34th pentad. The thermal difference then crosses zero around the 60th pentad. In late conversion years, the turning from negative to positive of the thermal difference occurs around the 15th pentad, which is similar to in early conversion years. However, the maximum value of only 295 W m^{-2} occurs in the 38th pentad. The thermal difference turns negative in the 56th pentad, which is four pentads in advance of that in early conversion years. The most significant distinction between early and late conversion is the maximum value in summer.

6.2 *Large-scale circulation effects*

To further study the influence of the early and late conversion of the thermal difference between SA and SIO on the outbreak time of the ISM, we analyze the timing of the establishment of the South Asian high (SAH) over the TP and the modal conversion of the Mascarene high (MH), and the circulation anomalies at 850 hPa.

The conversion of vertical velocity over the TP and SIO region represents the establishment of the ascending and descending branches of the ISM. From the perspective of circulation, it reflects the formation of upper-level high pressure over the TP and its surrounding regions, namely, the shift/establishment of the SAH to over the TP, and the formation of low-level pressure over the Mascarene region (the conversion of the MH from winter mode to summer mode). Based on the MH area index (MHAI) defined by Cui and Yang (2005), we obtain a multi-year annual mean MHAI of 140.45, which is used as a critical criterion in this study to determine the MH modal conversion. If the MHAI is larger than 140.45, the MH is regarded as being in its summer mode; otherwise, it is in its winter mode. Meanwhile, following Zhang (2016), the shift of the SAH to the TP is determined if the northernmost 1660 gpdm at 100 hPa reaches north of 30°N. Table 1 lists the establishment times of the SAH over the TP and the modal conversion times of the MH in early and late years of SA–SIO thermal difference conversion. It is clear that both the shift and establishment of SAH are earlier than normal in late years and later than normal in early years. This is consistent with the changes in the time of vertical velocity reversal and the ISM outbreak.

The above analysis focuses on the components of the ISM. In fact, the ISM is most significant in the 850-hPa wind field. For this reason, we further analyze the circulation at 850 hPa in April during the early and late years of thermal difference conversion. The anomalous circulation at 850 hPa in April for early conversion years is shown in Fig. 12a. The data indicate that anomalous southerlies occur over the Indian Peninsula, which are favorable for convective precipitation with increased water vapor transport from the Arabian Sea and BOB, but unfavorable for an increase in sensible heat flux; Indochina is under the control of an anticyclonic anomaly, which is unfavorable for the development of convective activities; anomalous easterlies cover the entire northern Indian Ocean region; anomalous northerlies are found over Somalia; and cyclonic circulation anomalies occur over the Mascarene region in the SIO, which suppresses the intensification of high pressure and is thus unfavorable

Table 1. Timing of the establishment of the SAH over the TP and the modal conversion of MH in early and late years of thermal difference conversion

	Timing of SAH establishment	Timing of MH modal conversion
Early years	Pentad 29.4	Pentad 9
Late years	Pentad 28.8	Pentad 5.6

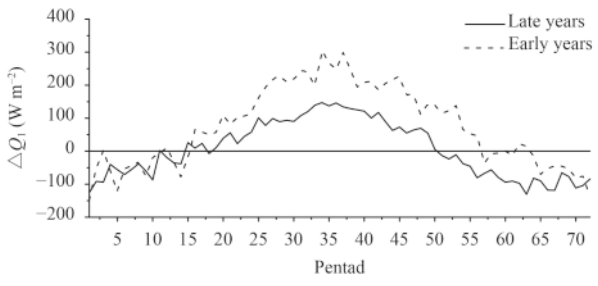

Fig. 11. The multi-year annual atmospheric heat source difference (ΔQ_1; W m^{-2}) between the TP and SIO in early and late conversion years from 1948 to 2013.

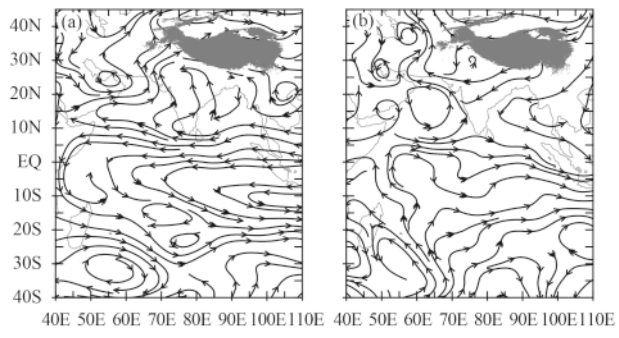

Fig. 12. Abnormal circulation (m s^{-1}) at 850 hPa in the (a) early and (b) late conversion years of the thermal difference.

for the outbreak of monsoon. In the late years of thermal difference conversion (Fig. 12b), the Indian Peninsula and Indochina are under the control of anomalous northerlies, which is unfavorable for water vapor transport but favorable for increases in sensible heat flux; anomalous cyclonic circulation occurs over the Arabian Sea; anomalous westerlies are found in the SIO; and anticyclonic anomalies cover the Mascarene region in the Southern Hemisphere, which is favorable for the intensification of high pressure and the outbreak of monsoon. Figure 13 shows the WYI conversion in early and late thermal difference conversion years. In early years, the WYI turns positive later than normal; in late years, it turns positive earlier than normal. From Table 1 and Figs. 12 and 13, the components of the ISM system, the anomalous circulation at 850 hPa, and the summer monsoon outbreak index, all indicate that in early years of thermal difference conversion, the outbreak of the ISM is later than normal, and vice versa.

The WYI has some capacity to explain the difference between the upper and lower levels of the troposphere in early and late conversion years. However, to explain this difference further, we show in Fig. 14 the April monthly mean vorticity distribution at 200 and 850 hPa in early and late conversion years. In early conversion years, there are two strong negative vorticity centers over the Arabian Peninsula and the east of the Indochina Peninsula at 200 hPa. At the same level, there is a positive vorticity center over the continent north of 30°N and the east of Madagascar. At 850 hPa, negative centers appear over the Arabian Peninsula, Indian Peninsula, Indochina Peninsula, and SIO. The equatorial area is covered by positive vorticity at the same level. Generally, in early conversion years, a barotropic structure appears over the continent north of 30°N, Indian Peninsula, and Indochina Peninsula. On the other hand, a baroclinic structure appears

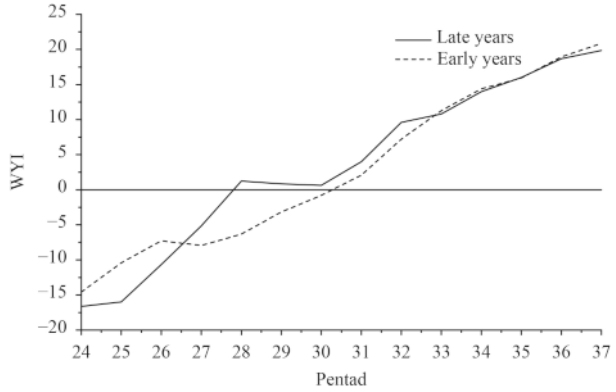

Fig. 13. The WYI (Webster–Yang index) conversion time in early and late years of the thermal difference conversion.

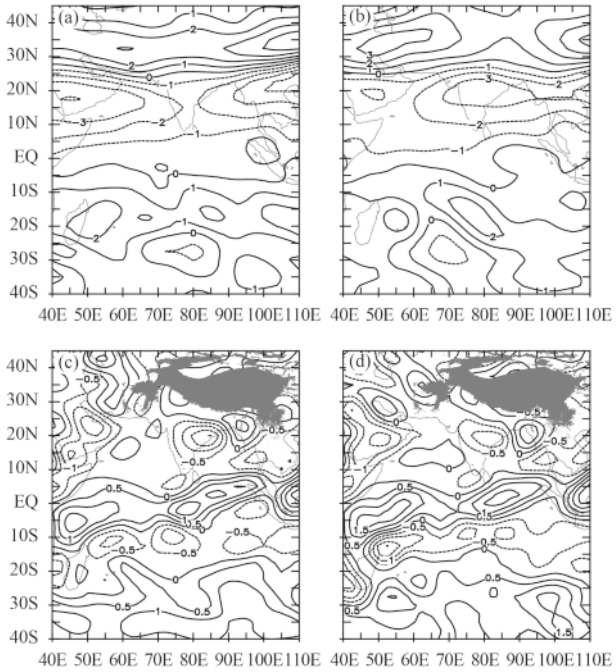

Fig. 14. The April mean vorticity distribution (10^5 s^{-1}) in (a, c) early and (b, d) late years of thermal difference conversion at (a, b) 200 hPa and (c, d) 850 hPa.

over the equatorial Indian Ocean and SIO. However, in late conversion years, the northern continent in the Northern Hemisphere still shows positive vorticity at 200 hPa. A strong negative vorticity center covers from the Indian Peninsula to Indochina Peninsula at the same level. The SIO is also covered by positive vorticity, but the center shifts to the central SIO. At 850 hPa, the Arabian Peninsula, Indochina Peninsula, and part of the Indian Peninsula are controlled by negative vorticity. The most intensive positive center is over the equatorial Indian Ocean, and negative vorticity presents over the Indian Ocean at about 10°S. In general, in late conversion years, a barotropic structure appears over the continent of the Northern Hemisphere, Arabian Peninsula, Indochina Peninsula, and part of the Indian Peninsula. A baroclinic structure is found over the Indian Ocean region at about 10°S and the equator. Overall, at 200 hPa, the distribution of vorticity follows apositive–negative–positive pattern in the meridional direction. However, the differences in the vorticity distribution between early and late years manifest mainly in the locations of high strength centers. The characteristics of distribution and strength are similar.

7. Conclusions

In the present study, the spatial distribution and temporal variability of the atmospheric heat source in the

SA–SIO region are analyzed, with a focus on the temporal variability and vertical distribution of the thermal difference between SA and the SIO. Composite analysis is also applied. The results indicate that large differences exist in the establishment time of the ascending and descending branches of the ISM between early and late years of SA–SIO thermal difference conversion. Combined with the changes and evolution of each component of the ISM, the mechanisms by which the thermal differences influence the outbreak of the ISM are explored. The effects of the planetary-scale meridional thermal difference across the TP–Indian Ocean region on the outbreak of the ISM and the underlying mechanisms are revealed. The key findings can be summarized as follows.

(1) The intraseasonal variability of the atmospheric heat source is significant over SA and the TP, but less so over the SIO. SA is a distinct heat source in summer and a heat sink in winter. The SIO region is a strong heat sink in summer, but is not a distinct heat source in winter. In spring, the distribution of the atmospheric heat source is characterized by transitional features before the outbreak of the summer monsoon. In spring, there is a temporary sequence of increased AHSS over the Northern Hemispheric continent. Because of its special topographic characteristics, the TP is highly sensitive to the seasonal variation of solar radiation. Consequently, the TP's AHSS increases faster than that of the subcontinental region of SA.

(2) The SA–SIO thermal difference and the TP–SIO thermal difference both show great intraseasonal variability. Their variational features are similar to those of the thermal effects of SA and the TP. The outbreak time of the ISM lags behind the time of thermal conversion by about 15 pentads. From the vertical distribution of the atmospheric heat source, it is found that the heat source decreases with height over both the TP and SA, with large differences in the heating effect among various levels. However, the vertical distribution of the heat source in southern India is opposite to that in the TP and SA, which first decreases with height and then increases with height. Similarly, the SA–SIO thermal difference also first decreases with height, and then increases with height. The thermal difference is most significant in the surface layer, and turns negative at upper levels. Analysis of the interannual variability suggests that the time when the SA–SIO thermal difference turns positive is highly negatively correlated with the outbreak time of the ISM. The thermal difference conversion time presents significant interannual variability, whereas the interannual variability of the outbreak time of the ISM is not that significant. The physical process by which the SA–SIO thermal difference influences the ISM outbreak is as follows. After the thermal difference turns positive in SA, the near-surface heat center drives ascending motion, and the negative thermal difference center creates descending motion. It is these vertical air motions that comprise the pre-monsoon circulation cell. The ascending branch gradually builds above the TP after the negative thermal difference center disappears. Therefore, the ISM's vertical meridional circulation establishes after the 30th pentad, and the ISM outbreak occurs.

(3) Early or late SA–SIO thermal difference conversion has substantial impacts on the outbreak of the ISM. Analysis of thermal forcing effects indicates that in years of early (late) thermal difference conversion, complete thermal conversion at each individual level of the atmosphere is later (earlier) than normal above the TP and SIO. As a result, complete vertical velocity reversal above the TP and SIO occurs later (earlier) than normal in response to the heating effect that appears later (earlier) than normal. Correspondingly, the ascending branch above the TP and the descending branch over the SIO, which are two important components of the meridional circulation of the ISM, also establish later (earlier) than normal, leading to later (earlier) than normal ISM outbreak. From the perspective of circulation, the establishment of the SAH in the TP and the conversion of the MH from its winter mode to summer mode both occur later (earlier) than normal in early (late) thermal difference conversion years. Meanwhile, both the circulation pattern at 850 hPa and the ISM index indicate that the outbreak of the ISM is later (earlier) than normal in early (late) thermal difference conversion years. However, the difference in the vorticity distribution between the upper and lower troposphere is manifested in the locations of the strong vorticity centers in early and late conversion years.

Acknowledgments. The authors would like to acknowledge the data providers, NCEP, for the NCEP–NCAR data, which are available at http://www.esrl.noaa.gov/psd/data/gridded/data.ncep.reanalysis.html. We also thank Prof. Shihua Lyu and Prof. Shigong Wang for their advice.

REFERENCES

Chen, L. X., and W. L. Li, 1981: Summer atmospheric heat budget in the Asian monsoon region. *Corpus of National Conference on Tropical Summer Monsoon* (*Volume One*). People's Press of Yunnan Province, Kunming, 18–101. (in Chinese)

Chen, L. X., and W. L. Li, 1982: Monthly structure of atmospheric heat source in Asian monsoon area. *Corpus of National Conference on Tropical Summer Monsoon* (*Volume Two*).

People's Press of Yunnan Province, Kunming, 246–258. (in Chinese)

Cui, J., and X. Q. Yang, 2005: The variation of Mascarene high and its relationship with ENSO. *Scientia Meteor. Sinica*, **25**, 441–449. (in Chinese)

Ding, Y. H., and K. Murakami, 1994: *Asian Monsoon*. China Meteorological Press, Beijing, 263 pp. (in Chinese)

He, J. H., Q. Li, J. Wei, et al., 2007: Reinvestigations on the East Asian subtropical monsoon and tropical monsoon. *Chinese J. Atmos. Sci.*, **31**, 1257–1265. (in Chinese)

He, J. H., H. M. Xu, S. S. Zhong, et al., 2011: *The Character of Atmospheric Heat Sources in Tibetan Plateau and Its Effects and Possible Mechanisms*. China Meteorological Press, Beijing, 243 pp. (in Chinese)

Jiang, N. B., and H. B. Luo, 1993: Intraseasonal variations of the atmospheric heat sources and moisture sinks over Asian monsoon region. Part I: Heat sources. *J. Trop. Meteor.*, **9**, 299–307. (in Chinese)

Kumar, S., T. Prasad, and A. L. Agrawal, 1999: A synoptic-climatic study of the onset of southwest monsoon over Mumbai. Proceedings of the Indian Academy of Sciences—Earth and Planetary Sciences, 108, 321–326.

Li, W. L., and L. X. Chen, 1983: Structure of the mean circulation and the heat budget in July over Asia. *Acta Meteor. Sinica*, **41**, 43–55. (in Chinese)

Liu, B. Q., Y. M. Liu, G. X. Wu, et al., 2015: Asian summer monsoon onset barrier and its formation mechanism. *Climate Dyn.*, **45**, 711–726, doi: 10.1007/s00382-014-2296-0.

Luo, H. B., and M. Yanai, 1984: The large-scale circulation and heat sources over the Tibetan Plateau and surrounding areas during the early summer of 1979. Part II: Heat and moisture budgets. *Mon. Wea. Rev.*, **112**, 966–989, doi: 10.1175/1520-0493(1984)112<0966:TLSCAH>2.0.CO;2.

Luo, M. X., and K. S. Zhang, 1991: Numerical experiment on the effects of the large scale topography and diabatic heating on the formation of East Asian monsoon and Indian monsoon circulations. *Scientia Atmospherica Sinica*, **15**, 41–52. (in Chinese)

Pan, J., and C. Y. Li, 2006: Comparison of climate characteristics between two summer monsoon troughs over the South China Sea and India. *Chinese J. Atmos. Sci.*, **30**, 377–390. (in Chinese)

Ramage, C. S., 1971: *Monsoon Meteorology*. Academic Press, 190 pp.

Wang, B., and Z. Fan, 1998: The choice of South Asian summer monsoon indices. *East Asian Monsoon and Chinese Storms*. China Meteorological Press, Beijing, 170–183. (in Chinese)

Wang, T. M., and G. X. Wu, 2008: Land–sea thermal contrast over South Asia and its influences on tropical monsoon circulation. *J. Trop. Meteor.*, **24**, 37–43. (in Chinese)

Webster, P. J., and S. Yang, 1992: Monsoon and ENSO: Selectively interactive systems. *Quart. J. Roy. Meteor. Soc.*, **118**, 877–926, doi: 10.1002/(ISSN)1477-870X.

Wu, G. X., and Y. M. Liu, 2000: Thermal adaptation, overshooting, dispersion, and subtropical anticyclone. Part I: Thermal adaptation and overshooting. *Chinese J. Atmos. Sci.*, **24**, 433–446. (in Chinese)

Wu, G. X., Y. Guan, T. M. Wang, et al., 2011: Vortex genesis over the Bay of Bengal in spring and its role in the onset of the Asian summer monsoon. *Science China (Earth Sciences)*, **54**, 1–9.

Xu, Z. F., and Y. F. Qian, 2006: Moist potential vorticity index of Indian monsoon and its relationship with climate in China. *Acta Meteor. Sinica*, **64**, 760–769. (in Chinese)

Yanai, M., C. F. Li, and Z. S. Song, 1992: Seasonal heating of the Tibetan Plateau and its effects on the evolution of the Asian summer monsoon. *J. Meteor. Soc. Japan*, **70**, 319–351.

Ye, D. Z., and Y. X. Gao, 1979: *Tibetan Plateau Meteorology*. Science Press, Beijing, 278 pp. (in Chinese)

Yim, S. Y., B. Wang, J. Liu, et al., 2014: A comparison of regional monsoon variability using monsoon indices. *Climate Dyn.*, **43**, 1423–1437, doi: 10.1007/s00382-013-1956-9.

Zhang, J., 2016: The relationship between South Asian high and the Tibetan Plateau monsoon. Ph. D. dissertation, Atmosphere Academy, Chengdu University of Information Technology, Chengdu, China, 13–17. (in Chinese)

Tech & Copy Editor: Zhirong CHEN
Language Editor: Colin SMITH